Progress In Oceanography
June 2021, Volume 194 Pages 102570 (14p.)
https://doi.org/10.1016/j.pocean.2021.102570
https://archimer.ifremer.fr/doc/00700/81199/

An observing system simulation experiment for Indian Ocean surface pCO2 measurements

Valsala Vinu [1, *], Sreeush M. G. [1, 5, 6], Anju M. [1, 2], Sreenivas Pentakota [1], Tiwari Yogesh K. [1],
Chakraborty Kunal [3], Sijikumar S. [4]

[1] Minist Earth Sci, Indian Inst Trop Meteorol, Pune, Maharashtra, India.
[2] Andhra Univ, Coll Sci & Technol, Dept Meteorol & Oceanog, Visakhapatnam, Andhra Pradesh, India.
[3] Minist Earth Sci, Indian Natl Ctr Ocean Informat Serv, Hyderabad, India.
[4] Vikram Sarabhai Space Ctr, Space Phys Lab, Thiruvananthapuram, Kerala, India.
[5] Inst Basic Sci, Ctr Climate Phys, Busan 46241, South Korea.
[6] Pusan Natl Univ, Busan 46241, South Korea.

* Corresponding author : Vinu Valsala, email address : valsala@tropmet.res.in

Abstract :

An observing system simulation experiment (OSSE) is conducted to identify potential locations for making surface ocean pCO2 measurements in the Indian Ocean using the Bayesian Inversion method. As of the SOCATv3 release, the pCO2 data is limited in the Indian Ocean. To improve our modeling of this region, we need to identify where and what observation systems would produce the most good or benefit for their cost. The potential benefits of installing pCO2 sensors in the existing RAMA and OMNI moorings of the Indian Ocean, the potential of Bio-Argo floats (with pH measurements), and the implementation of the ship of opportunity program (SOOP) for underway sampling of pCO2 are evaluated. A cost function of dissolved inorganic carbon as a model state vector and CO2 flux mismatch as the source of error is minimized, and the basin-wide CO2 flux uncertainty reduction is estimated for different seasons. The maximum flux uncertainty reduction achievable by installing pCO2 sensors in the existing RAMA and OMNI moorings is limited to 30% during different seasons. One may consider that around 20 Bio-Argos are still the right choice over installing mooring based pCO2 sensors and achieve uncertainty reduction up to 50% with additional benefit of profiling the sub-surface upto 1000 & ndash;2000 m. However, a single track SOOP has the potential to reduce the uncertainty by approximately 62%. This study identifies vital RAMA and OMNI moorings and SOOP tracks for observing Indian Ocean pCO2.

Plain Language Summary.

Surface ocean partial pressure of CO2 (pCO2) information is vital for estimating sea-to-air CO2 exchanges. This parameter is least available from the Indian Ocean as compared to other global tropical and southern oceans. There has been no effort made so far to measure surface ocean pCO2 in the Indian Ocean with routine monitoring such as by mounting instruments to moorings or by underway sampling via any ship of opportunity program. Therefore there is a considerable demand to start pCO2 observations in the Indian Ocean. However, one key question that emerges is where to deploy pCO2 instruments in the Indian Ocean to learn the most with limited resources. This study addresses this question with inverse modeling techniques. The study finds that the existing moorings of the Indian Ocean are capable of hosting pCO2 sensors, and data from those are useful to reduce the uncertainty in the surface sea-to-air CO2 flux estimation by a quarter magnitude. In contrast, the Bio-Argo floats with pH sensors, and the ship of opportunity underway sampling of pCO2 may benefit from reducing the same up to 50% and 62%, respectively.

Highlights

► OSSE is done for Indian Ocean (IO) pCO_2 using RAMA + OMNI moorings, Bio-Argo floats and SOOP ship-tracks. ► pCO_2 data from moorings and ship-tracks are tested for air-sea CO_2 flux inversions. ► The maximum CO_2 flux uncertainty reduction (UR) with potential pCO_2 data is found. ► IO-UR with pCO_2 data from moorings and ship-tracks are 30% and 62%, respectively. ► Ship-track pCO_2 is more efficient than the mooring pCO_2 data in CO_2 flux inversion.

Keywords : Observing System Simulation Experiment, (OSSE), RAMA mooring, OMNI mooring-Ship of Opportunity (SOOP)

1. Introduction

The ocean plays a vital role in mitigating global climate change by sequestering ~30% of anthropogenically emitted carbondioxide (CO_2) per year (Sabine et al., 2004; Valsala and Maksyutov, 2010; Le Quéré et al., 2018; Friedlingstein et al., 2019; Gruber et al., 2019). In the absence of this sink, the accumulation of human-made CO_2 in the atmosphere could have been amplified by a corresponding magnitude, and global warming would have been much more accelerated. The global ocean has taken up nearly 165 ± 20 petagrams of carbon (PgC) emitted since the pre-industrial era (Le Quéré et al., 2018). The contemporary global ocean CO_2 sink is estimated to be 2.5 ± 0.6 Pg C yr^{-1} (Friedlingstein et al., 2019).

Tropical Indian Ocean (IO) alone contributed to sinking 16.6 ± 5.1 petagrams anthropogenic carbon, amounting a 16% of the global total ocean sink (Sabine et al., 2004). The recent synthesis of the Indian Ocean (north of 40°S) sea-to-air CO_2 flux suggests an annual mean (median) CO_2 uptake of -0.37 ± 0.06 Pg C yr^{-1} based on models and a sink of -0.24 ± 0.12 PgC yr^{-1} based on observational estimates, for a period of 1990-2010 (Table-3, Sarma et al., 2013). Observation-based estimates of sea-to-air CO_2 fluxes show that the Indian Ocean (from 40°S to 30°N) is a carbon sink of -0.17 ± 0.12 Pg C yr^{-1} as constructed from 1980-2014 neural network-based data product of Landschutzer et al. (2016). On the other hand, variational data assimilation of available surface ocean partial pressure of CO_2 (pCO_2) observations into a biogeochemical model suggests a sink of -0.28 ± 0.18 Pg C yr^{-1} for the same region as constructed from 1980-2009 (Valsala and Maksyutov, 2010).

The divergence among various observational estimates of the Indian Ocean sea-to-air CO_2 fluxes mostly arises from the lack of pCO_2 data need for the CO_2 flux calculations. Although the Surface Ocean CO_2 Atlas (SOCATv3-2020) database consists of 28 million quality controlled surface ocean pCO_2 measurements available from 1970 to 2019, the Indian Ocean (30°E-130°E, 40°S-30°N) shares only 0.8 million, hardly representing 2.8% of the total quality-controlled global pCO_2 data, especially for north of 30°S (Pfeil et al., 2013, Bakker et al., 2016, Rödenbeck et al., 2015, Bakker et al., 2020). Despite being the third-largest global ocean, the inadequate data coverage of the Indian Ocean hampers the accurate renditions and budgeting of its carbon cycle. It is perhaps not much felt in the seasonal cycle (Takahashi et al., 2009, 2014). Indeed, it affects deducing the subtle interannual and decadal variability (Bates et al., 2006, Rödenbeck et al., 2015, Landschutzer et al., 2016, Sarma et al., 2013, Valsala et al., 2012, 2020). There has been no effort made to sample pCO_2 by underway sampling using volunteer commercial ships in the Indian Ocean, unlike in the north Pacific and Atlantic (Zeng et al., 2014). It leaves a significant data gap in the Indian Ocean, especially north of 30°S (Bakker et al., 2020).

The surface ocean pCO_2 can be measured by instruments mounted to moorings or attached to the hull of ships in case of underway sampling (Pierrot et al., 2009; Takeshita et al., 2018). Considering the spatiotemporal diversity of the Indian Ocean physical and biogeochemical characteristics (Schott and McCreary, 2001; Prasanna Kumar et al., 2001; 2007; Wiggert et al., 2005; 2006; Levy et al., 2007; Murtugudde et al., 2007; McCreary et al., 2009; Sarma, 2002; 2013) and limited availability of resources to make direct observations, consideration must be given to determine: (a) which existing moorings in the Indian Ocean where instruments can be installed to make pCO_2 measurements most cost-effectively? (b) which ship-track should be selected for the underway sampling under the voluntary ship of opportunity programs (SOOP) so that the data obtained are optimal to constrain the Indian Ocean sea-to-air CO_2 fluxes in inversion based estimates (Jacobson et al., 2007; Valsala and Maksyutov, 2010; Mukherjee et al., 2011; Khatiwala et al., 2013; Steinkamp and Gruber, 2013, 2015; Sreeush et al., 2019). Intensive ocean observations of pCO_2 and more atmospheric tower observations are required to improve the models (Sarma et al., 2013, Wanninkhof et al., 2019, Nalini et al., 2019).

Indian Ocean Observing System (IndOOS) is the sustained observing system for the Indian Ocean, a network operated and supported by various national agencies and coordinated internationally under the Global Ocean Observing System framework by the CLIVAR/IOC-GOOS Indian Ocean Region Panel. A detailed observing system simulation experiment (OSSE) has been done for the physical variables of the Indian Ocean as part of IndOOS.1 programs in the early 2000s (a group of publications in the special issue of J. Climate, Vol.50, 2007). The net result of this effort is the installation of Research Moored Array for African-Asian-Australian Monsoon Analysis and Prediction (RAMA) in the Indian Ocean (Vecchi and Harrison, 2005; Ballabrera-Poy et al., 2007; Sakov and Oke, 2008; Oke and Schiller, 2007; McPhaden et al., 2009). IndOOS has updated its priorities into actionable recommendations for future observing system components and has put forwarded recommendations for an effective observational program of the Indian Ocean (Beal et al., 2020a,b).

Among the IndOOS.2 recommendations for the 2020-30 frameworks, the Bio-Argos are expected to be increased by 200 in number (Beal et al., 2019 and their Figure ES.1, Hood et al., 2020, Wanninkhof et al., 2019). Other two notable recommendations are: (a) to initiate Moored Autonomous pCO_2 systems (MAPCO2) and biogeochemical measurements at RAMA locations and (b) to establish SOOP-CO_2 measurements in the southern Indian Ocean (IX21, Hood, et al., 2020). Therefore an OSSE for Indian Ocean pCO_2 measurements based on RAMA moorings and based on various ship tracks of the Indian Ocean (Tournadre 2004) and thereby to substantiate the IndOOS.2 recommendations are the need of the hour. This topic has not been attempted in any previous studies to the best of our knowledge, except for the extreme southern part of the Indian Ocean (Majkut et al., 2014). In another notable study, Ford (2021) tested the proposed Bio-Argo arrays (Gray et al., 2018) in improving the simulated pCO_2 of the global oceans.

Despite the strong recommendations under IndOOS.2 in place, only one of the existing RAMA moorings in the entire array is equipped with sensors for making surface ocean pCO_2 measurements (located at 90°E and 15°N) in the central Bay of Bengal popularly known as the Bay of Bengal Ocean Acidification Mooring (BOBOA; Sutton et al. 2016, 2017). BOBOA quality controlled pCO_2 is available from 2013 to the present but with data gaps in 2014-15 and 2017-18. It is to be noted that this observation system had been installed considering logistical convenience. However, BOBOA data's benefits in constraining the Bay of Bengal sea-to-air CO_2 fluxes as a basin have not been evaluated. Ye et al. (2019) utilized this data to study the high-frequency variability in pCO_2 and the role of Bay of Bengal cyclones in surface ocean carbon fluxes.

In addition to RAMA mooring, another major Indian Ocean mooring program initiated by the Government of India is the Ocean Moored buoy Network for the Northern Indian Ocean, popularly known as OMNI buoy network (Venkatesan et al., 2013). Under this program, seven moorings are operational in the Bay of Bengal, and another five are operational in the Arabian Sea. They are also potential sites for pCO2 observations in the north Indian Ocean.

The Indian Ocean is also home to major global commercial shipping routes. It hosts two major shipping channels: Malacca Strait in the east and Suez Canal in the west. Estimated global energy transportation is about 2.4 million barrels of oil per day, representing 5.5% of world oil transport, taken through these channels (Valsala and Roy, 2014). Tournadre (2014) and Figure 1 there show the significant ship-routes in the Indian Ocean as inferred from altimetry data sensed by instruments mounted onboard satellites by NASA. Therefore, the Indian Ocean has the potential to host a SOOP for the underway sampling of pCO_2. In this context, the emerging question is 'what is the best track to start SOOP in the Indian Ocean? We note here that in IndOOS.2, one of its recommendations includes establishing SOOP-CO_2 measurements in the southern Indian Ocean (IX21) repeat track (Beal et al., 2020), whereas other potential SOOP tracks remain unexplored.

The present study addresses the gap mentioned in the above areas by answering the following key questions: (a) what are the optimal mooring locations of RAMA and OMNI arrays for making pCO_2 measurements? (b) what is the potential of Bio-Argo floats (including pH sensors) in replacing moored buoy sensors in the future, and (c) what are the potential SOOP ship-tracks in the Indian Ocean for measurements of surface ocean pCO_2? These measurements will lead to a better estimate of sea-to-air CO_2 fluxes for the Indian Ocean. The remaining part of the paper is organized as follows. Section-2 introduces the model and methodology adopted.

Section-3 discusses each mooring's ranking in the RAMA and OMNI array to initiate surface ocean pCO2 measurements and discuss the OSSE done for various ship-tracks to find optimal SOOP tracks in the Indian Ocean. The significant recommendations are made in Section-4.

2. Model, Data, and Methodology

2.1. Physical and Biogeochemical model and Data

The study utilizes the Ocean Tracer Transport Model (OTTM; Valsala et al., 2008) coupled with the Ocean Carbon-cycle Model Intercomparison Project (OCMIP-II) biogeochemistry (Najjar and Orr, 1998) and with a modified biological parameterization for net community compensation depth (Sreeush et al., 2018). More details of physical design, ocean re-analysis data used to run OTTM, the coupled OCMIP-II biogeochemistry modules with modified parameterization, and the model carbon cycle validation are given in Sreeush et al. (2018, 2019) therefore will not be repeated here.

2.2. Methodology

We use the Bayesian inversion method to identify the best locations for making observations of surface ocean pCO_2. In this case, we are minimizing the following cost function constructed with sea-to-air CO_2 flux errors and mismatches in dissolved inorganic carbon (DIC) between model and observations:

$$J = (GS_0 - D)^T C_d^{-1}(GS_0 - D) + (S - S_o)^T C_{S_o}^{-1}(S - S_o) \qquad (1)$$

GSo is the model response vector corresponding to the observation, 'D,' taken as DIC in the model. C_{S_o} represents prior sea-to-air flux uncertainty of CO_2. C_d contains a combination of both observational (C_{obs}) and model (C_{mod}) errors. S_0 and S are the prior and posterior sea-air CO_2

fluxes, respectively. Here the observed pCO_2 is converted to DIC using abiotic pump routines of OCMIP-II (Najjar and Orr, 1998), and the corresponding errors in the conversions are embedded into C_d (see section 2.2.2). The Bayesian theory states that the above cost function is minimum if the flux vector S_0 assumes the optimized form (Tarantola, 2004; Lewis et al., 2006);

$$S = S_o + \left(G^T C_d^{-1} G + C_{S_o}^{-1}\right)^{-1} G^T C_d^{-1} (D - G S_o) \tag{2}$$

Here we note that the DIC, pCO_2, and sea-to-air CO_2 fluxes behave differently in carbonate chemistry routines (Sarmiento and Gruber, 2006). In the model, the prognostic variable is DIC and pCO_2 is diagnostic to that. Therefore, to constrain the model with observations, we opt to convert pCO_2 data into DIC using abiotic routines of OCMIP-II. It is an effective method and has proven capacity in reducing surface ocean pCO_2 biases in variational assimilation (Valsala and Maksyutov, 2010). The errors we expect in this conversion are mainly arising from temperature, salinity, and Alkalinity (ALK). Here we note that the temperature and salinity data are utilized from the re-analysis of ocean data, which have been used to run this model; therefore, the errors are expected to be minimal. The past studies (Sreeush et al., 2018, 2019) show that the model has reasonable pCO_2 and sea-to-air CO_2 fluxes across all the biomes considered in this study due to a fine-tuning in the OCMIP-II parameters, which further takes care of the simulated DIC and ALK. Therefore the total error in converting the pCO_2 into DIC is expected to be minimal, and still, we encapsulate an equivalent error of ± 2.5 μatm expected as an upper bound in the conversion into our observational error matrix as detailed in Section 2.2.2.

2.2.1. *G*-matrix

The *G*-matrix represents the model response function in terms of DIC to a given perturbation in the S_o vector (i.e., sea-to-air CO_2 fluxes in this case). The Indian Ocean was divided into eight important biomes, as in Sreeush et al. (2019). The area integrated sea-to-air CO_2 fluxes of each of these regions are perturbed each month by a constant value of one Pg C yr^{-1} sink. Here we note that the magnitude of perturbation has little influence on the G-matrix's deduced elements because G-matrix normalizes DIC concentrations to the given flux perturbation of a particular region. The model was simulated from 1996 to 2005 (termed as SENS after this). The perturbations were given only for the month of interest but during all years of the simulation from 1996 to 2005. For eight oceanic regions and for 12 months (from January to December), there were a total of 96 SENS runs. The G-matrix consists of model state variable differences (here we kept as surface ocean DIC) between the control run (CTRL), and SENS runs sampled from the model at mooring locations for the last year of the simulation. Here we note that the period of simulation (1996-2005) is not sensitive in the inversion as it is only used to get the sensitivity of the model to a given perturbation flux in each oceanic region in each month.

2.2.2. C_d matrix

This matrix contains the sum of both observational (C_{obs}) and model (C_{mod}) DIC errors at the observation location. In this setup, the observed pCO_2 is assumed as converted to DIC using the solubility pump routines of OCMIP-II. In this conversion, the C_{obs} includes an equivalent RMSE in DIC while converting an 'observational' pCO_2 with a maximum assumed error of ± 2.5 µatm. The conversion of pCO_2 to DIC also encapsulates the errors in the dependent variables such as sea surface temperature, ALK, phosphate (PO_4), silicate, and other minor ions. This calculation was done using model outputs spanning from 1960 to 2009, and the RMSE of reconstructed DIC is utilized for C_{obs}.

2.2.3. C_{S_o} matrix

This matrix consists of flux variance-covariance of area integrated fluxes between each oceanic region and each month. It has been calculated from the monthly sea-to-air CO_2 fluxes of assimilated data from 1980 to 2009 (Valsala and Maksyutov, 2010). The diagonal elements are the variances of the seasonal cycle of the regional (i.e., R1 to R8) integrated sea-to-air CO_2 fluxes, whereas the off-diagonal elements represent the co-variances of the seasonal cycle of fluxes between each oceanic region.

The OSSE is based on the assumption that no real observations (*D*) are required to determine the utility of observation from a particular mooring location, Bio-Argo float, or ship-track in reducing the estimated surface flux uncertainty in the inverse modeling. The first part in the second term of R.H.S. of Equation (2) is the posterior flux uncertainty (C_s) if the observations are available from given locations and for a given prior flux uncertainty of C_{S_o}. It is estimated as:

$$C_s = \left(G^T C_d^{-1} G + C_{S_o}^{-1}\right)^{-1} \qquad (3)$$

Therefore the percentage uncertainty reduction (UR) in the flux estimation can be quantified as:

$$UR = \left[\frac{trace(\boldsymbol{C}_s) - trace(\boldsymbol{C}_{s_o})}{trace(\boldsymbol{C}_{s_o})}\right] \times 100 \qquad (4)$$

(in %) where 'trace' represents the sum of diagonal elements of the respective matrices.

2.2.4. Incremental Optimization

To rank all moorings of RAMA and OMNI array for installation of pCO2 sensor and evaluate the potential Bio-Argo floats and Indian Ocean ship tracks for SOOP, an incremental optimization method as described in Nalini et al. (2019) is utilized. Suppose there are 'n' moorings in RAMA and OMNI. They all are considered 'candidate set' suitable for installing pCO_2 sensors, further assuming that observations from each of these 'candidate sets' as available, the UR of Indian Ocean sea-to-air CO_2 flux individually contributed by each of these moorings is quantified. The mooring with maximum UR is then moved to a 'base set,' and the candidate set is reduced to ‘n – 1'. Further, a second mooring from the 'candidate set' is added to the 'base set,' and the UR due to a combination of two moorings is estimated. The candidate with maximum UR is then permanently moved to the 'base-set' so that 'candidate set' is reduced to ‘n – 2' and 'base set' is grown to 2. The above process is repeated until all the 'candidate set' got added to the 'base set.' The rank of each mooring is the same as the sequence it gets added to the ‘base set.’

In this study total of 43 moorings (31 RAMA moorings and 12 OMNI moorings) are considered. Similarly, one Bio-Argo float per every 10^ox10^o region in the Indian Ocean is deployed in the model and carried out an incremental optimization for the floats just as done for the RAMA and OMNI buoys. A total of 38 Bio-Argo floats were distributed at equal distances from each other. We have considered data from a particular location (i.e., the center of each 10^ox10^o box) as available via Bio-Argo for all 12 months in a year. Over a month scale, the Argos are not going to drift so much. However, it may drift over a year. Nevertheless, for a uniform deployment of Argo, they may replace the positions so that the frequency of data from a particular locality could be maintained over time to sample the relatively uniform open ocean conditions of the upper ocean carbon cycle. The choice of 38 floats is made as a case study targeting the expansion of Indian Ocean Bio-Argo with pH sensors in the next ten years. Although the recommendation of IndOOS.2 is to achieve 200 Bio-Argo floats in total by 2030 (Hood et al., 2020), we assumed roughly 20% of them would have pH sensors in them. We note here that there is no other Bio-Argo in the Indian Ocean with pH sensors (except for recently launched in the sout-western Indian Ocean) and therefore anticipating a total of 200 Bio-Argos all with pH sensors in the next ten years is a bit too optimistic. To find the optimal ship-track for SOOP, a set of potential ship-routes of the Indian Ocean is selected based on Tournadre (2014). The UR by each of the ship-tracks is separately calculated (no incrementally), and all tracks are ranked accordingly.

3. Results

Figures 1 and 2 show the seasonal mean surface sea-to-air CO_2 fluxes and surface DIC concentrations simulated by the model represented as a mean constructed from the simulation period of 1996-2005 (from CTRL). The essential seasonal features of surface ocean sea-to-air CO_2 fluxes are reproduced well in the model compared to observational estimates of Takahashi et al. (2014). The perennial source of tropical Indian Ocean CO_2 is reproduced in the model well with intense emissions from the western Arabian Sea during boreal summer (Poisson et al., 1993, Sabine et al., 2000, Valsala and Maksyutov, 2013). The seasonal DIC is also comparable with observations from Takahashi et al., (2014).

3.1. Bioprovinces used for regional CO_2 flux inversions

Figure 3 shows the eight oceanic bio-provinces identified in Sreeush et al. (2019) based on the homogeneity in the seasonal variances of community compensation depth and the subsequent variability in net primary and export production. The variability in surface ocean pCO_2 can cascade through the ocean's biological and solubility pumps and infer the community compensation depth, which is an integral part of these two pumps. Among these eight regions, R1 to R6 straddles most of the RAMA and OMNI array (Figure 3a). However, there are no moorings to represent R7 and R8 (Figure 3a). It will have implications in the inversion such that the UR for the region R7 and R8 will be minimal and affect the overall UR in the posterior fluxes of the basin. On the other hand, the major ship tracks cover all these oceanic regions (Figure 3b). Figure 4 shows the seasonality of the area integrated sea-to-air CO_2 fluxes of eight oceanic regions used in this study and shown from the assimilated sea-to-air CO_2 flux of Valsala and Maksyutov (2010). A detail of the seasonal evolution of area integrated sea-to-air CO_2 fluxes in Figure 4 is given in Sreeush et al. (2019); therefore will not be repeated here.

3.2. Elements of G-matrix, Model and Observational errors

Figure 5 shows the total response in the surface ocean DIC (μmol kg^{-1}) due to a given perturbation in each oceanic region of Figure 3 as in Section 2.2.1. The figure represents the RMSE of DIC difference between CTRL and SENS runs in the *G*-matrix simulations. This figure is produced using the last year of model-simulated data. The total response is spread widely in the Indian Ocean and reached a distance far away from the individual regions, albeit with much less spread in the case of R7 and R8. R1 has maximum sensitivity close to the northeast coast of the Arabian Sea, where the mixed layer is controlled by coastal currents, entrainment, and convective deepening (Shankar et al., 2016; Singh et al., 2019). R2 has the maximum surface signature in DIC due to weak mixing in the relatively fresh waters of the Bay of Bengal (Valsala et al., 2018). R7 and R8 also have significant signals in the surface ocean, implying weaker mixing in the oligotrophic part of the gyre where the solubility pump dominates the upper ocean's carbon cycle (Valsala et al., 2012). The other regions have moderate sensitivity in the surface ocean DIC. The maxima of RMSE in DIC in Figure 5 could indicate a potential location for observing the surface ocean pCO_2. For instance, the R2 has maximum RMSE close to central BoB, where it tentatively matches with existing BOBOA pCO_2 mooring (Sutton et al., 2017). However, all other such locations may not necessarily correspond to a RAMA or OMNI mooring location. Therefore, an inversion based on Equation 1-4 is apparent for retrieving the optimal number of RAMA and OMNI moorings to capture the maximum DIC signals of Figure 5.

Figure 6 shows the corresponding RMSE used for the C_{mod} calculations. Ideally, it is the same as Figure 5 except for the perturbations given in each oceanic region. The model error (C_{mod}) is calculated by 'propagating' the CO_2 flux uncertainty of each oceanic region of each month to the mooring locations via simulation from 1996 to 2005. It is the same as we did for the *G*-matrix, but with perturbations given as standard deviations of C_{So}. The maximum value of C_{mod} is close to ±2 μmol kg^{-1}.

Figure 7 shows the C_{obs} seasonal cycle for the selected mooring location from the central Arabian Sea (65°E, 15°N), as an example. The seasonality in error is a function of the ocean's ambient surface state, which are involved in the calculations of abiotic OCMIP-II carbon solubility pump calculation. The error here implies the observational error for each month, which also encapsulates the conversion error from pCO_2 to DIC in the model. Here the conversion of

pCO_2 to DIC depends on temperature, ALK, salinity, and other minor ions. The first three are highly seasonal, and the conversion error is also seasonal in this case (Broullón et al., 2019). It is ideal to have a broader error representation in the inversion so that we understand each station's limitation in providing 'insightful' pCO_2, in this case, for constraining surface ocean sea-to-air CO_2 fluxes.

3.3. OSSE for RAMA and OMNI moorings

The ranking of each RAMA and OMNI moorings in the total UR of the prior fluxes is calculated separately for four seasons: March-May (MAM), June-September (JJAS), October-November (ON), and December-February (DJF). The seasons are identified following the known characteristics of the Indian monsoon, which has significant control over the Indian Ocean biogeochemistry (Wiggert et al., 2005). Figure 8 shows the seasonal rankings of RAMA and OMNI moorings for surface ocean pCO_2 measurements in the Indian Ocean as obtained from our OSSE. The ranks are indicated as colors with deep blue (red) representing a highly (slightly) impactful mooring location as per this OSSE. Figure 10a shows the percentage of UR achieved by making use of all 43 moorings. The UR reaches saturation within the first 15 moorings. The UR varies with seasons under varying surface ocean dynamics and carbon pump strength in the Indian Ocean (Sreeush et al., 2018). A maximum UR of 30% is obtained during DJF, JJAS, and ON with 15 moorings, while 23% is obtained during MAM. It is noted that the rankings change the positions seasonally. However, a cluster of the first few ranks is relatively consistent among various seasons. This fact encourages us to proceed with pCO_2 sensor installation in these moorings as they are consistent across various seasons. The heterogeneity of rankings among seasons indicates the complicated physical and dynamic biogeochemical nature of the Indian

Ocean. We have also found a ranking of all RAMA moorings done with the annual mean response of '*G*' matrices (figure not shown). In this case, the maximum UR is 25%, which is very close to the mean of all UR in four seasonal OSSE. The first six ranks' locations are reasonably consistent with those obtained for seasonal OSSE in Figure 8.

3.4. OSSE for Bio-Argo floats

Figure 9 shows a similar ranking obtained for the Bio-Argo floats. Bio-Argo floats are distributed equally at a 10° x10° resolution in the Indian Ocean; therefore, they are spread widely across various biomes. The total UR by Bio-Argo floats is as large as 50%, with a total number of floats less than 20 (Figure 10b). The regional patterns of ranks obtained with Bio-Argo floats are consistent with those of moorings. However, due to relative changes in the location of Bio-Argo floats considered here compared to the moorings, the ranks are also relatively shifted. A significant consensus is that the equatorial Indian Ocean ranks are relatively weaker in both moorings and Bio-Argo floats in the present OSSE. Considering the relatively smooth operations and implimentaiton of Bio-Argo floats, one may consider that around 20 Bio-Argos are still the right choice over installing mooring based pCO_2 sensors inferred in terms of UR (Figure 10a, b). However, a caveat is that the Bio-Argo floats can detect the pH while mooring can directly measure the pCO_2. Calculating the surface ocean pCO_2 from float pH has uncertainty contributions from the pH sensor, the alkalinity estimate, and carbonate system equilibrium constants, resulting in a relative standard uncertainty in pCO_2 of 2.7% (or 11 μatm at pCO_2 of 400 μatm, Williams et al., 2017).

3.5. OSSE for Ship tracks

Figure 11a-b shows the ranking of ship tracks for January and July, respectively. Figure 11c-d shows the UR during January and July for ten ship tracks considered in this study. Unlike moorings, the ship-track optimizations are done for individual ship-tracks separately (not the incremental optimization with one ship tracks over the other) with the view that SOOP cannot initiate in multiple tracks as it is not practical. It is assumed that the data collected within a month from each of these tracks represent the entire duration of the month, which is not a caveat because commercial ship takes less than ten days to cross the Indian Ocean in all major tracks used in the analysis. The maximum UR by a single track is somewhat close to 65%. The results are consistent among seasons and shown here for two contrasting months (i.e., January and July). Compared to the mooring, SOOP's advantage is that SOOP covers the entire ocean and contributes significantly to reducing UR from all identified oceanic regions considered in this study. Individually, the first and second ranked ship-tracks reduce the uncertainty closely by 62%, and the first four ranked tracks are the same for both January and July. The result shows that SOOP is far more effective at reducing UR in this OSSE (~62%) than utilizing time-series stations (~30%).

A consolidated diagram of moorings selected based on the ranks within the Arabian Sea, Bay of Bengal, equatorial Indian Ocean, and south subtropical Indian Ocean for all four seasons is provided as the 'best set' in Figure 12. The inner-circle (outer) circle shows whether the mooring belongs to a rank-range of 1-2 (3-4) as re-ordered for each sub-basin above. Different seasons are indicated in different colors. If the ranks are standard during multiple seasons, the circle shares the colors accordingly.

In conclusion, based on OSSE, a total of 24 moorings and four ship-tracks are highly recommended as per this study (Figure 12). Locations important for the moorings are six each in the Arabian Sea and Bay of Bengal, while the moorings in the southwest equatorial Indian Ocean (i.e., close to Seychelles -Chagos thermocline ridge region) also rank high for pCO_2 representativeness. Surprisingly, the moorings in the southwest equatorial Indian Ocean ranking high for pCO_2 measurements (i.e., close to the Seychelles-Chagos thermocline ridge region). It could be because the south equatorial current (S.E.C.) passes and diverges at the western continental boundary through this dynamically significant region. 70% of the S.E.C. turns north at the western boundary (Valsala and Ikeda, 2007) and spreads through the north Indian Ocean. The seawater pCO_2 measured from this region may have a higher value in constraining the north Indian Ocean CO_2 fluxes due to the fast-flowing western boundary currents, potentially spreading through considerable distances before equilibrating with atmospheric pCO_2 (Sarmiento and Gruber, 2006).

The study also put forward four essential SOOP tracks based on the first two ranks in OSSE (shown as black stars in Figure 12) and also based on busy shipping routes but ranks within the first six in OSSE (shown as cyan stars in Figure 12). The ship traffic analysis shows a global fourfold growth between 1992 and 2012, the largest increase observed in the Indian Ocean and the Chinese seas reflecting the world trade change (Tournadre, 2014). Notably, the track starting from the South African coast also shares the track with the projected repeat track of IX21(until the south Madagascar Islands) as in the IndOOS.2 recommendations (Beal et al., 2020a,b).

4. Conclusion

Using Bayesian inversion theory and incremental optimization technique and utilizing a global ocean biogeochemical model, for the first time, we have optimized the locations of RAMA and OMNI moorings, Bio-Argo floats, and commercial ship tracks for making measurements of pCO_2 in the Indian Ocean that would improve the overall knowledge of carbon flux in this basin. The cost function is minimized in such a fashion that the observations of pCO_2 from these moorings, floats, or ship tracks are optimal for the maximum reduction in the CO_2 flux uncertainty of the Indian Ocean in an ocean inversion framework. The results show that due to the spatio-temporal variability of Indian Ocean physical and biogeochemical dynamics and its strong dependency on seasonality, multiple mooring locations must be equipped with pCO2 sensors to capture its variability throughout the year.

Ship-track measurements of underway pCO_2 in SOOP are far more efficient in constraining Indian Ocean CO_2 fluxes than time-series data from fixed moorings. The maximum flux uncertainty reduction achievable by installing pCO_2 sensors in the existing RAMA and OMNI mooring is limited to 30% in different seasons. However, a single track SOOP can reduce the current uncertainty by approximately 62%, albeit with OSSE has been conducted during January and July. SOOP covers a larger area, while mooring represents only selected stationary locations. Given that the equilibration time scale of surface ocean pCO_2 with the atmosphere is few weeks to months, the pCO_2 instruments attached to mooring may not capture the carbon information of far away distances. However, ships can measure all the Indian Ocean regions over a shorter timescale, providing invaluable knowledge. On the other hand, considering the relatively smooth operation and implementation of Bio-Argo floats, one may consider that around 20 Bio-Argos are still the right choice over installing mooring based pCO_2 sensors.

However, a caveat is that the Bio-Argo floats can detect the pH while mooring can directly measure the pCO_2. While Bio-Argos can give a profile of pH up to 1000-2000m range in the ocean that is additional merit over SOOP. This study provides first-ever guidelines for initiating future pCO_2 measurements in the Indian Ocean.

5. Acknowledgment

The authors acknowledge the support from the Ministry of Earth Sciences (MoES), Govt. of India, and its various programs operating at IITM. All the model simulations are performed in the HPC facility of MoES. SMG acknowledges the support of the Institute for Basic Science (IBS), Republic of Korea, under IBS-R028-D1

6. Data Availability:

GFDL re-analysis data is taken from https://www.gfdl.noaa.gov/ocean-data-assimilation/
GLODAP data is taken from https://www.nodc.noaa.gov/ocads/oceans/GLODAPv2/
WOA-2013 data is taken from https://www.nodc.noaa.gov/OC5/woa13/
Takahashi et al., (2009) data is taken from https://www.nodc.noaa.gov/ocads/oceans/LDEO_Underway_Database/
Boundary layer wind data for sea-to-air flux is taken from https://psl.noaa.gov/data/gridded/data.ncep.reanalysis2.html
The model outputs used in this analysis are available at https://zenodo.org/record/3833776#.XsO330QzbIU .

7. References

Bakker, D. C. E., Pfeil, B., Landa, C. S., et al. (2016), A multi-decade record of high quality *f*CO_2 data in version 3 of the Surface Ocean CO_2 Atlas (SOCAT), Earth Syst. Sci. Data, 8, 383–413, https://doi.org/10.5194/essd-8-383-2016.

Bakker, Dorothee C. E.; et al., (2020). Surface Ocean CO2 Atlas Database Version 2020 (SOCATv2020) (NCEI Accession 0210711). [indicate subset used]. NOAA National Centers for Environmental Information. Dataset. https://doi.org/10.25921/4xkx-ss49. Accessed [date].

Ballabrera-Poy, J., E. Hackert, R. Murtugudde, and A.J. Busalacchi, 2007: An Observing System Simulation Experiment for an Optimal Moored Instrument Array in the Tropical Indian Ocean. *Journal of Climate,* **20**, 3284–3299, https://doi.org/10.1175/JCLI4149.1

Bates, N. R., A. C. Pequignet, and C. L. Sabine, 2006. Ocean carbon cycling in the Indian Ocean: 1. Spatiotemporal variability of inorganic carbon and sea-to-air CO2 gas exchange, Global Biogeochem. Cycles, 20, GB3020, doi:10.1029/2005GB002491.

Beal, L. M., Vialard, J., Roxy, M. K. and lead authors 2019: Executive Summary. IndOOS-2: A roadmap to sustained observations of the Indian Ocean for 2020-2030. CLIVAR-4/2019, GOOS-237, 8 pp. doi: https://doi.org/10.36071/clivar.rp.4-1.2019

Beal, L., M., J. Vialard, M. K. Roxy, 2020a. IndOOS-2: A Consolidated and Enhanced Indian Ocean Observing System for the Next Decade In "The Recent Decadal Review (2020-2030) of the Indian Ocean Observing System (IndOOS-2) and its Outcomes". (Yu L., Ed), Clivar Exchanges, N° 78, Feb 2020, DOI: 10.36071/clivar.78.2020

Beal, et, al., A roadmap to IndOOS-2: Better observations of the rapidly-warming Indian Ocean, *Bull. Amer. Meteor. Soc***.** (2020b), https://doi.org/10.1175/BAMS-D-19-0209.1

Broullón, D., Pérez, F. F., Velo, A., Hoppema, M., Olsen, A., Takahashi, T., Key, R. M., Tanhua, T., González-Dávila, M., Jeansson, E., Kozyr, A., and van Heuven, S. M. A. C., (2019), A global monthly climatology of total alkalinity: a neural network approach, Earth Syst. Sci. Data, 11, 1109-1127, https://doi.org/10.5194/essd-11-1109-2019.

Ford, D.: Assimilating synthetic Biogeochemical-Argo and ocean colour observations into a global ocean model to inform observing system design (2021), Biogeosciences, 18, 509–534, https://doi.org/10.5194/bg-18-509-2021

Friedlingstein, P., Jones, M. W., O'Sullivan, et al.,(2019), Global Carbon Budget 2019, Earth Syst. Sci. Data, 11, 1783–1838, https://doi.org/10.5194/essd-11-1783-2019, 2019.

Gray, A., K.S. Johnson, S.M Bushinsky, S.C. Riser, J.L. Russell, L.D. Talley, R. Wanninkhof, N.L. Williams, and J.L. Sarmiento. (2018), Autonomous biogeochemical floats detect significant carbon dioxide outgassing in the high-latitude Southern Ocean, Geophys. Res. Lett., 45. 10.1029/2018GL078013

Gruber, N., D. Clement, B. R. Carter, R.A. Feely, S. Van Heuven, M. Hoppema,M. Ishii,R. M. Key,A. Kozyr, S. K. Lauvset, C. Lo Monaco,J. T. Mathis, A. Murata, A Olsen, F. F. Perez,C. L. Sabine, T. Tanhua, R. Wanninkhof (2019), The oceanic sink for anthropogenic CO_2 from 1994 to 2007, Science, Vol. 363, Issue 6432, pp. 1193-1199, DOI: 10.1126/science.aau5153.

Hood, R. R., P. G. Strutton, and J. D. Wiggert, 2020. Physical and Biogeochemical Processes and Interactions in the Indian Ocean. In "The Recent Decadal Review (2020-2030) of the Indian Ocean Observing System (IndOOS-2) and its Outcomes". (Yu L., Ed), Clivar Exchanges, N° 78, Feb 2020, DOI: 10.36071/clivar.78.2020

Jacobson, A. R., Fletcher, S. E. M., Gruber, N., Sarmiento, J. L., and Gloor, M. (2007), A joint atmosphere-ocean inversion for surface fluxes of carbon dioxide: 1. Methods and global scale fluxes. *Global Biogeochemical Cycles, 21, GB1019,*https://doi.org/10.1029/2005GB002556

Khatiwala, S., Tanhua, T., Mikaloff Fletcher, S., Gerber, M., Doney, S. C., Graven, H. D., … Sabine, C. L. (2013), Global ocean storage of anthropogenic carbon. *Biogeosciences,*10,2169-2191, https://doi.org/10.5194/bg-10-2169-2013.

Landschützer, P., Gruber, N., & Bakker, D. C. E. (2016). Decadal variations and trends of the global ocean carbon sink. *Global Biogeochemical Cycles*, *30*(10), 1396–1417. https://doi.org/10.1002/2015GB005359

Le Quéré, C., Andrew, R. M., Friedlingstein, P., et al., (2018), Global Carbon Budget 2018, Earth Syst. Sci. Data, 10, 2141–2194, https://doi.org/10.5194/essd-10-2141-2018

Lévy, M., Shankar, D., André, J. M., Shenoi, S. S. C., Durand, F., & de Boyer Montégut, C. (2007). Basin-wide seasonal evolution of the Indian Ocean's phytoplankton blooms.*Journal of Geophysical Research: Oceans*, *112*(12). https://doi.org/10.1029/2007JC004090.

Lewis, J. M., S. Lakshmivarahan., and S. K. Dhall (2006), Dynamic Data assimilation: a least squares approach, Cambridge University Press, ISBN9780521851558.

Majkut J. D, Carter BR, Frölicher TL, Dufour CO, Rodgers KB, Sarmiento JL. (2014) An observing system simulation for Southern Ocean carbon dioxide uptake. Phil. Trans. R. Soc. A 372: 20130046. http://dx.doi.org/10.1098/rsta.2013.0046

McCreary, J., Murtugude, R., Vialard, J., Vinayachandran, P., Wiggert, J. D., Hood, R. R., Shankar, D., Shetye, S., (2009), Biophysical processes in the Indian Ocean, Indian Ocean Biogeochemical Processes and Ecological Variability., 9 – 32, Online ISBN:9781118666364, doi: 10.1029/GM185.

McPhaden, M.J., G. Meyers, K. Ando, Y. Masumoto, V.S. Murty, M. Ravichandran, F. Syamsudin, J. Vialard, L. Yu, and W. Yu, (2009), RAMA: The Research Moored Array for African–Asian–Australian Monsoon Analysis and Prediction, *Bulletin of theAmerican* 410 *Meteorological Society,* 90(4), 459 – 480, https://doi.org/10.1175/2008BAMS2608.1

Mukherjee, C., Kasibhatla, P. S., & West, M. (2011).Bayesian statistical modeling of spatially correlated error structure in atmospheric tracer inverse analysis.*Atmospheric Chemistry and Physics*, *11*(11), 5365–5382. https://doi.org/10.5194/acp-11-5365-2011

Murtugudde, R., Seager, R., &Thoppil, P. (2007).Arabian Sea response to monsoon variations. *Paleoceanography*, *22*(4), 1–17. https://doi.org/10.1029/2007PA001467

Najjar, R. G., & Orr, J. C. (1998).Design of OCMIP-2 simulations of chlorofluorocarbons, the solubility pump and common biogeochemistry.*Internal OCMIP Report*, 25. Retrieved from http://ocmip5.ipsl.fr/documentation/OCMIP/phase2/simulations/design.ps

Nalini, K., Sijikumar, S., Valsala, V., Tiwari, Y, K., Ramachandran, R (2019), Designing surface CO_2 monitoring network to constrain the Indian Land fluxes, *Atmospheric Environment*, 218, 117003, https://doi.org/10.1016/j.atmosenv.2019.117003

Oke, P.R. and A. Schiller, 2007: A Model-Based Assessment and Design of a Tropical Indian Ocean Mooring Array, *Journal of Climate,* 20, 3269–3283, https://doi.org/10.1175/JCLI4170.1

Olsen, A., Lange, N., Key, R. M., Tanhua, T., Bittig, H. C., Kozyr, A., Álvarez, M., Azetsu-Scott, K., Becker, S., Brown, P. J., Carter, B. R., Cotrim da Cunha, L., Feely, R. A., van Heuven, S., Hoppema, M., Ishii, M., Jeansson, E., Jutterström, S., Landa, C. S., Lauvset, S. K., Michaelis, P., Murata, A., Pérez, F. F., Pfeil, B., Schirnick, C., Steinfeldt, R., Suzuki, T., Tilbrook, B., Velo, A., Wanninkhof, R., and Woosley, R. J.,: (2020), An updated version of the global interior ocean biogeochemical data product, GLODAPv2.2020, Earth Syst. Sci. Data, 12, 3653-3678, https://doi.org/10.5194/essd-12-3653-2020, 2020.

Pfeil, B., et al, 2013. A uniform, quality controlled Surface Ocean CO2 Atlas (SOCAT), Earth Syst. Sci. Data, 5, 125-143, doi:10.5194/essd-5-125-2013, 2013.

Pierrot, D., C. Neill, K. Sullivan, R. Castle, R. Wanninkhof, H. Luger, T. Johannessen, A. Olsen, R. A. Feely, C. E. Cosca, (2009), Recommendations for autonomous underway pCO_2 measuring systems and data-reduction routines, *Deep Sea Research, pt II*, 56, 512 – 522, doi:10.1016/j.dsr2.2008.12.005.

Poisson, A., et al., (1993). Variability of sources and sinks of CO2 in the western Indian and southern oceans during the year 1991, J. Geophys. Res., 98(C12), 22759- 22778, doi:10.1029/93JC02501.

Prasanna Kumar, S., Nuncio, M., Ramaiah, N., Sardesai, S., Narvekar, J., Fernandes, V., & Paul, J. T. (2007).Eddy-mediated biological productivity in the Bay of Bengal during fall and spring intermonsoons.*Deep-Sea Research Part I: Oceanographic Research Papers*. https://doi.org/10.1016/j.dsr.2007.06.002

Prassana Kumar. S, Ramaiah. N, Gauns. M., Sarma V. V. S. S., Muraleedharan. P. M., RaghuKumar. S., Dileep Kumar., Madhupratap. M., (2001), Physical forcing of biological productivity in the Northern Arabian Sea during the Northeast Monsoon, *Deep Sea Res. Pt. II.,* 48, 1115-1126, doi:10.1016/S0967-0645(00)00133-8.

Rödenbeck, C., Bakker, D. C. E., Gruber, N., Iida, Y., Jacobson, A.R., Jones, S., Landschützer, P., Metzl, N., Nakaoka, S., Olsen, A., Park, G.-H., Peylin, P., Rodgers, K. B., Sasse, T. P., Schuster, U., Shutler, J. D., Valsala, V., Wanninkhof, R., Zeng, J., (2015), Data-based estimates of the ocean carbon sink variability - First results of the Surface Ocean pCO2 Mapping intercomparison (SOCOM). Biogeosciences 12: 7251-7278. doi:10.5194/bg-12-7251-2015

Sabine, C. L., Feely, R. A., Gruber, N., Key, R. M., Lee, K., Bullister, J. L., R. Wanninkhof, C.S. Wong., D. W. R. Wallace, B. Tilbrook, Frank J. Millero, T. Peng., A. Kozyr, T. Ono.,A. F. Rios (2004), The oceanic sink for anthropogenic CO_2 , *Science,* 305, 367 – 371, doi:10.1126/science.1097403.

Sabine, C. L., R. Wanninkhof, R. M. Key, C. Goyet, and F. J. Millero, (2000), Seasonal CO2 fluxes in the tropical and subtropical Indian Ocean, Mar. Chem., 72, 33-53. https://doi.org/10.1016/S0304-4203(00)00064-5.

Sakov, P. and P.R. Oke, 2008: Objective Array Design: Application to the Tropical Indian Ocean. *J. Atmos. Oceanic Technol.,* **25**,794–807, https://doi.org/10.1175/2007JTECHO553.1

Sarma, V. V. S. S. (2002). An evaluation of physical and biogeochemical processes regulating perennial suboxic conditions in the water column of the Arabian Sea. *Global Biogeochemical Cycles*, *16*(4), 29-1-29–11. https://doi.org/10.1029/2001gb001461

Sarma, V. V. S. S., Lenton, A., Law, R. M., Metzl, N., Patra, P. K., Doney, S., Lima, I. D., Dlugokencky, E., Ramonet, M., and Valsala, V. (2013), Sea–air CO_2 fluxes in the Indian Ocean between 1990 and 2009, *Biogeosciences,* 10, 7035-7052, https://doi.org/10.5194/bg-10-7035-2013.

Sarmiento, J. L., and Gruber, N. (2006), Ocean Biogeochemical Dynamics, Princeton University Press, New Jersey.

Schott, F. A., & McCreary, J. P. (2001), The monsoon circulation of the Indian Ocean. *Progress in Oceanography,* 51, 1-123, https://doi.org/10.1016/S0079-6611(01)00083-0.

Shankar, D., Remya, R., Vinayachandran, P.N., Chatterjee, A and Behera, A.,(2016). Inhibition of mixed-layer deepening during winter in the northeastern Arabian Sea by the West India Coastal Current. *ClimDyn* **47,** 1049–1072 (2016). https://doi.org/10.1007/s00382-471 015-2888-3.

Singh, S.**,** V. Valsala, A. G. Prajeesh, S. Balasubramanian, (2019). On the variability of Arabian Sea mixing and its energetics. Journal of Geophysical Research: Oceans,124. https://doi.org/10.1029/2019JC015334

Sreeush, M. G., Valsala, V., Halder, S., Pentakota, S., Prasad, K. V. S. R., Naidu, C. V., and Murtugudde, R., (2019), Biological production in the Indian Ocean upwelling zones: Part – II: Data based estimates of variable compensation depth for ocean carbon models via cyclo-stationary Bayesian inversion, *Deep Sea Res., Pt II,*https://doi.org/10.1016/j.dsr2.2019.07.007.

Sreeush, M. G., Valsala, V., Pentakota, S., Prasad, K. V. S. R., &Murtugudde, R. (2018). Biological production in the Indian Ocean upwelling zones - Part 1: Refined estimation via the use of a variable compensation depth in ocean carbon models. *Biogeosciences*,*15*(7), 1895–1918. https://doi.org/10.5194/bg-15-1895-2018

Steinkamp, K., and Gruber, N. (2013), A joint atmosphere-ocean inversion for the estimation of seasonal carbon sources and sinks, *Global Biogeochemical Cycles*, 27(3), 732– 745, https://doi.org/10.1002/gbc.20064.

Steinkamp, K., and Gruber, N. (2015).Decadal trends of ocean and land carbon fluxes from a regional joint ocean-atmosphere inversion, *Global Biogeochemical Cycles,*29(12), 2108–2126, https://doi.org/10.1002/2014GB004907.

Sutton, Adrienne J.; Sabine, Christopher L.; Dietrich, Colin; Maenner Jones, Stacy; Musielewicz, Sylvia; Bott, Randy; Osborne, John (2017). High-resolution ocean and atmosphere pCO2 time-series measurements from mooring Mooring BOBOA_90E_15N (NCEI Accession 0162473). [indicate subset used]. NOAA National Centers for Environmental Information. Dataset. https://doi.org/10.7289/v5h70d1k.

Sutton, A. J., Sabine, C. L., Feely, R. A., Cai, W. J., Cronin, M. F., McPhaden, M. J., et al. (2016). Using present-day observations to detect when anthropogenic change forces surface ocean carbonate chemistry outside preindustrial bounds. Biogeosciences, 13(17), 5065-5083. https://doi.org/10.5194/bg-13-5065-2016

Takahashi, T., Sutherland, S. C., Wanninkhof, R., Sweeney, C., Feely, R. A. and co-authors, (2009), Climatological mean and decadal changes in surface ocean pCO_2 and net sea-air CO_2 flux over the global oceans, *Deep Sea Research part II,* 56, 554–577, doi:10.1016/j.dsr2.2008.12.009.

Takahashi, T., S.C. Sutherland, D.W. Chipman, J.G. Goddard, Cheng Ho, T. Newberger, C. Sweeney, D.R. Munro, (2014). Climatological Distributions of pH, pCO2, Total CO2, Alkalinity, and CaCO3 Saturation in the Global Surface Ocean, and Temporal Changes at Selected Locations. Marine Chemistry. doi: 10.1016/j.jmarchem.2014.06.004.

Takeshita, Y., Johnson, K. S., Martz, T. R., Plant, J. N., & Sarmiento, J. L. (2018). Assessment of autonomous pH measurements for determining surface seawater partial pressure of CO_2 *.Journal of Geophysical Research: Oceans, 123*, 4003–4013. https://doi.org/10.1029/2017JC013387

Tarantola, A. (2004), Inverse Problem 498 Theory and Methods for Model Parameter Estimation.*Society for Industrial and Applied Mathematics*, ISBN: 978-0-89871-572-9, https://doi.org/10.1137/1.9780898717921.

Tournadre, J (2014), Anthropogenic pressure on the open ocean: The growth of ship traffic revealed by altimeter data analysis, *Geophysical Research Letters,* 41, 7924 – 7932, doi:10.1002/2014GL061786.

Valsala V. and M. Ikeda, (2007), Pathways and effects of the Indonesian Throughflow water in the Indian Ocean using Particle trajectory and Tracers in an OGCM. J. Climate,, 20, 2994-3017.

Valsala, K. V., Maksyutov, S., Ikeda, M., (2008), Design and Validation of an offline oceanic tracer transport model for a carbon cycle study, *Journal of Climate,* 21, 2752 – 2769, doi: 10.1175/2007JCLI2018.1.

Valsala, V., and Maksyutov, S. (2010), Simulation and assimilation of global ocean pCO_2 and sea-to-air CO_2 fluxes using ship observations of surface ocean pCO_2 in a simplified biogeochemical offline model. *Tellus, Series B: Chemical and Physical Meteorology,* 62: 821-840, https://doi.org/10.1111/j.1600-0889.2010.00495.x

Valsala, V., S. Maksyutov, and R. Murtugudde (2012), A window for carbon uptake in the southern subtropical Indian Ocean, Geophys. Res. Lett., 39, L17605, doi:10.1029/2012GL052857.

Valsala, V., and, S. Maksyutov, (2013), Interannual variability of the air–sea CO2 flux in the north Indian Ocean, Ocean Dynamics, DOI:10.1007/s10236-012-0588-7, 1-14

Valsala V. and C. Roy (2014), The Suez Canal, *Quarterly Newsletter of Ocean Society of India*, Pune Chapter, 1(2), ISSN 2394 – 1928.

Valsala, V., Singh, S., &Balasubramanian, S. (2018), A modeling study of interannual variability of Bay of Bengal mixing and barrier layer formation, *Journal of Geophysical Research: Oceans,* 123, 3962–3981, https://doi.org/10.1029/2017JC013637

Valsala, V., M. G. Sreeush, and K. Chakraborty, (2020), IOD impacts on Indian the Ocean Carbon Cycle, Journal of Geophysical Research, https://doi.org/10.1029/2020JC016485

Vecchi, G.A. and M.J. Harrison (2007), An Observing System Simulation Experiment for the Indian Ocean. *Journal of Climate,* 20, 3300–3319, https://doi.org/10.1175/JCLI4147.1

Venkatesan, R., V. R. Shamji, G. Latha, S. Mathew, R. R. Rao, A. Muthiah and M. A. Atmanand (2013), In situ ocean subsurface time-series measurements from OMNI buoy network in the Bay of Bengal, Current Science, Vol. 104, NO. 9, 10 MAY 2013

Wanninkhof, R., P. Pickers, A. Omar, A. J. Sutton, A. Murata, A. Olsen, B. Stephens, B. Tilbrook, D. Munro, D. Pierrot, G. Rehder, J. M. Santana-Casiano, J. Müller, J. A. Trinanes, K.

A. Tedesco, K. M. O'Brien, K. Currie, L. Barbero, M. Telszewski, M. Hoppema, M. Ishii, M. González-Dávila, N. R. Bates, N. Metzl, P. Suntharalingam, R. A. Feely, S. Nakaoka, S. K. Lauvset, T. Takahashi, T. Steinhoff, U. Schuster, 2019. A surface ocean CO2 reference network, SOCONET and associated marine boundary layer CO2 measurements. Frontiers in Marine Science, 6, 400, DOI:10.3389/fmars.2019.00400

Wiggert, J. D., Hood, R. R., Banse, K., Kindle, J. C., (2005), Monsoon-driven biogeochemical processes in the Arabian Sea, *Progress in Oceanography,* 65, 176-213, doi:10.1016/j.pocean.2005.03.008.

Wiggert. J. D., Murtugudde, R. G., Christian J. R., (2006), Annual ecosystem variability in the tropical Indian Ocean: results of a coupled bio-physical ocean general circulation model, *Deep Sea Research. Part. II,* 53, 644-676, doi:10.1016/j.dsr2.2006.01.027.
Zeng, J., Y. Nojiri, P. Landschützer, M. Telszewski, and S. Nakaoka, (2014), A Global Surface Ocean fCO_2 Climatology Based on a Feed-Forward Neural Network. *J. Atmos. Oceanic Technol.,* **31**, 1838–1849, https://doi.org/10.1175/JTECH-D-13-00137.1

Williams, N. L., L. W. Juranek R. A. Feely K. S. Johnson J. L. Sarmiento L. D. Talley A. G. Dickson A. R. Gray R. Wanninkhof J. L. Russell S. C. Riser Y. Takeshita, (2017), Calculating surface ocean pCO2 from biogeochemical Argo floats equipped with pH: An uncertainty analysis, Global Biogeochem. Cycles, 31, 591– 604, doi:10.1002/2016GB005541.

Ye, H., Sheng, J., Tang, D., Morozov, E., Kalhoro, M. A., Wang, S., & Xu, H. (2019). Examining the impact of tropical cyclones on sea-to-air CO2 exchanges in the Bay of Bengal based on satellite data and in situ observations. Journal of Geophysical Research: Oceans, 124, 555-576. https://doi.org/10.1029/2018JC014533

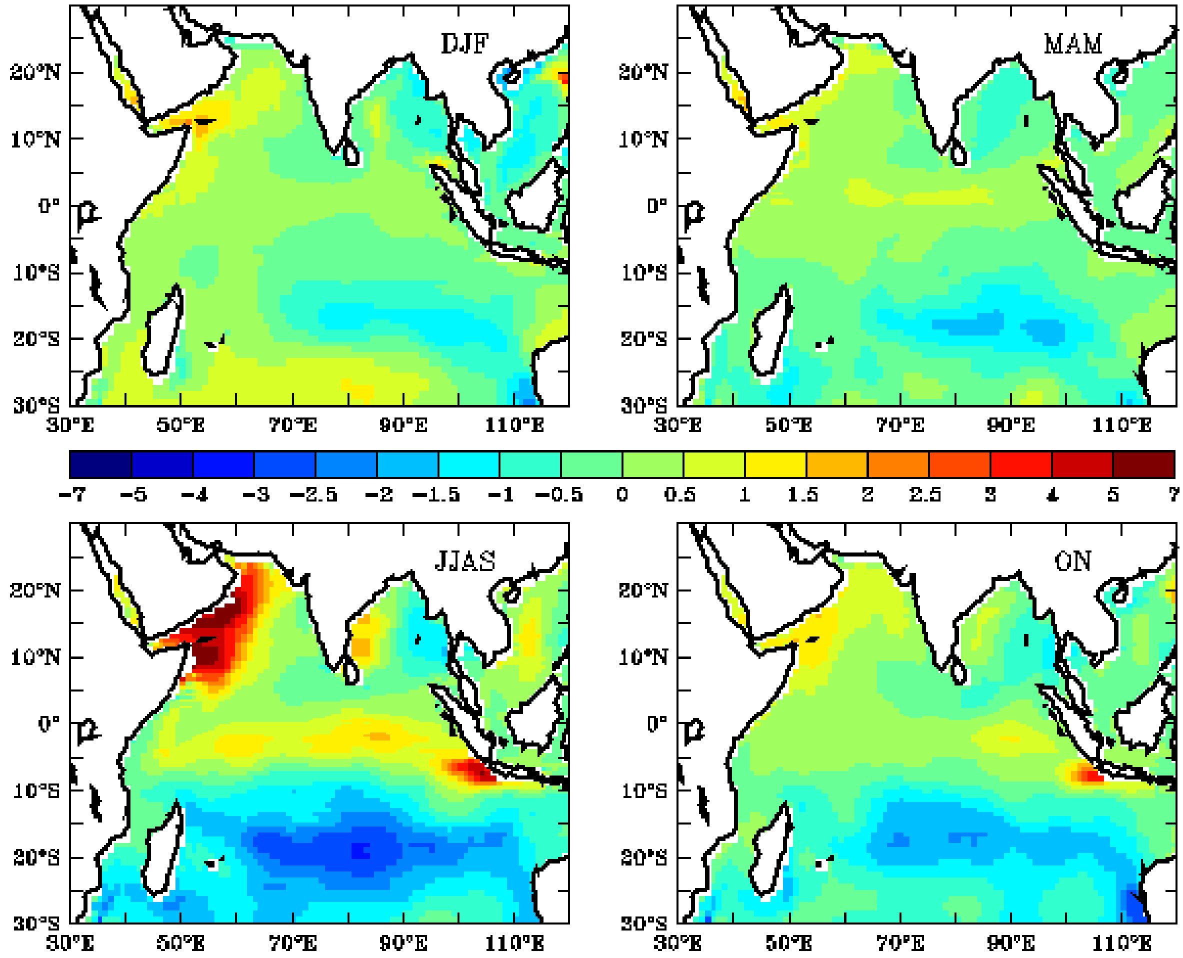

Figure 1: Seasonal mean sea-to-air CO_2 fluxes from the model shown as mole m^{-2} yr^{-1}.

804 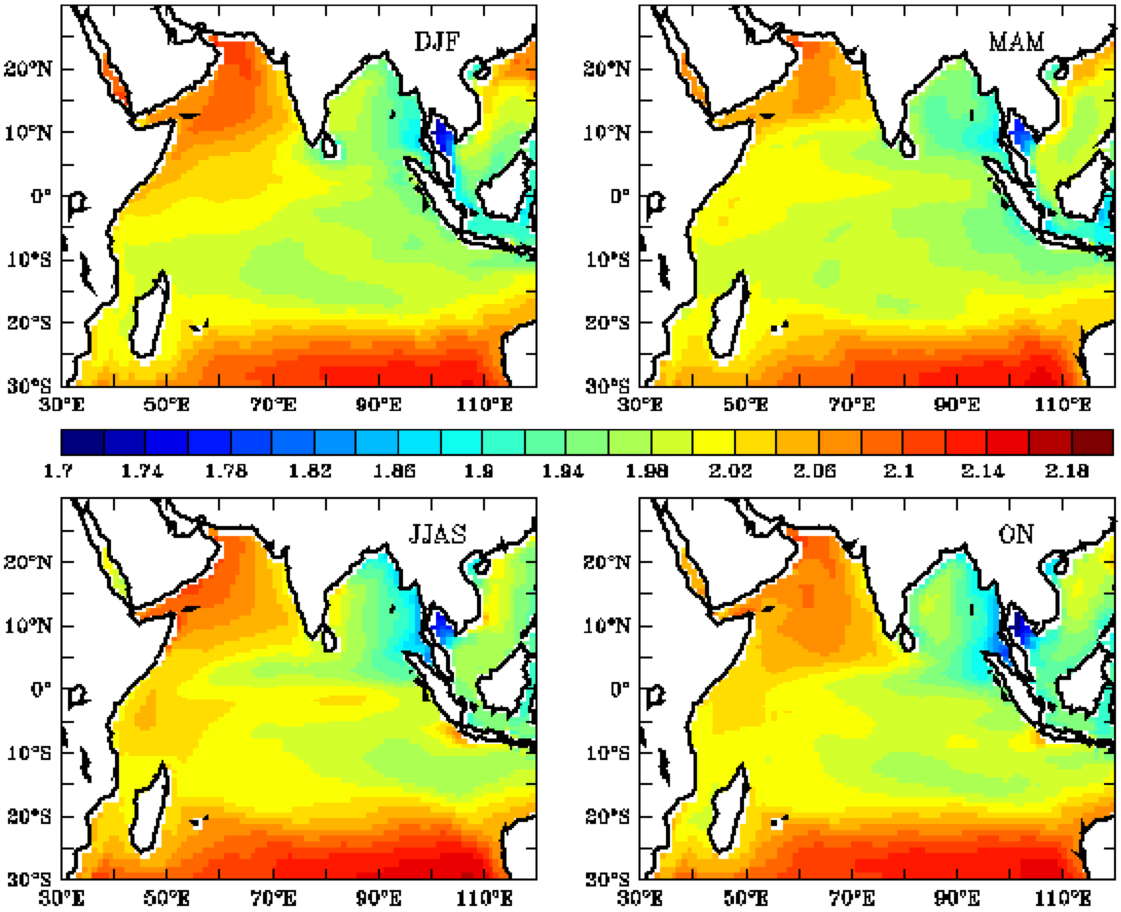

805

806 **Figure 2**: Seasonal mean surface ocean dissolved inorganic carbon (DIC) from the model shown

807 as mole m^{-3}

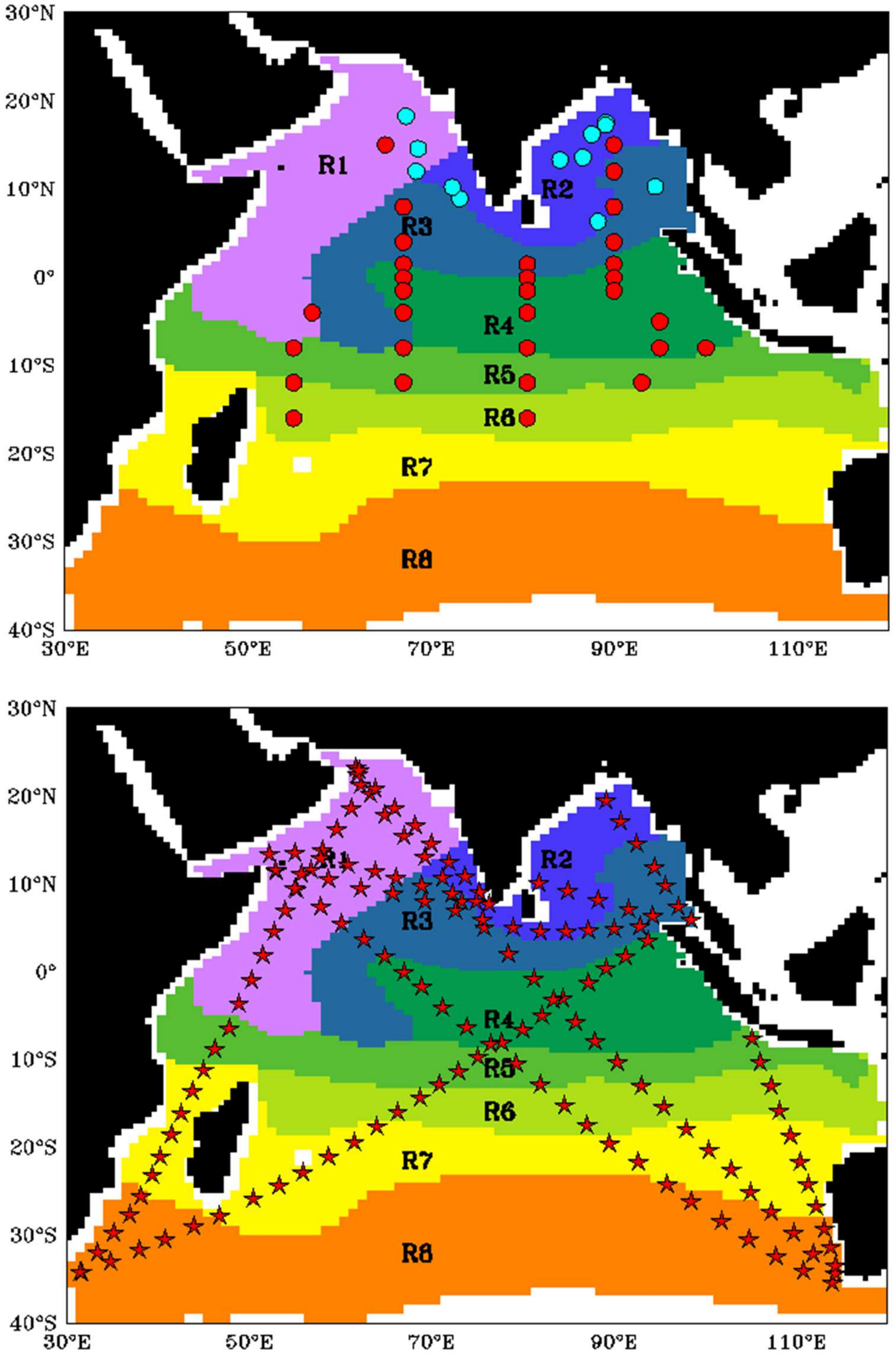

Figure 3: Eight oceanic bio-provinces (R1-R8) are denoted with different colors, as in Sreeush et al. (2019) overlaid with (a) RAMA (red) + OMNI (cyan) mooring locations (b) selected potential SOOP tracks based on satellite data of Tournadre (2014).

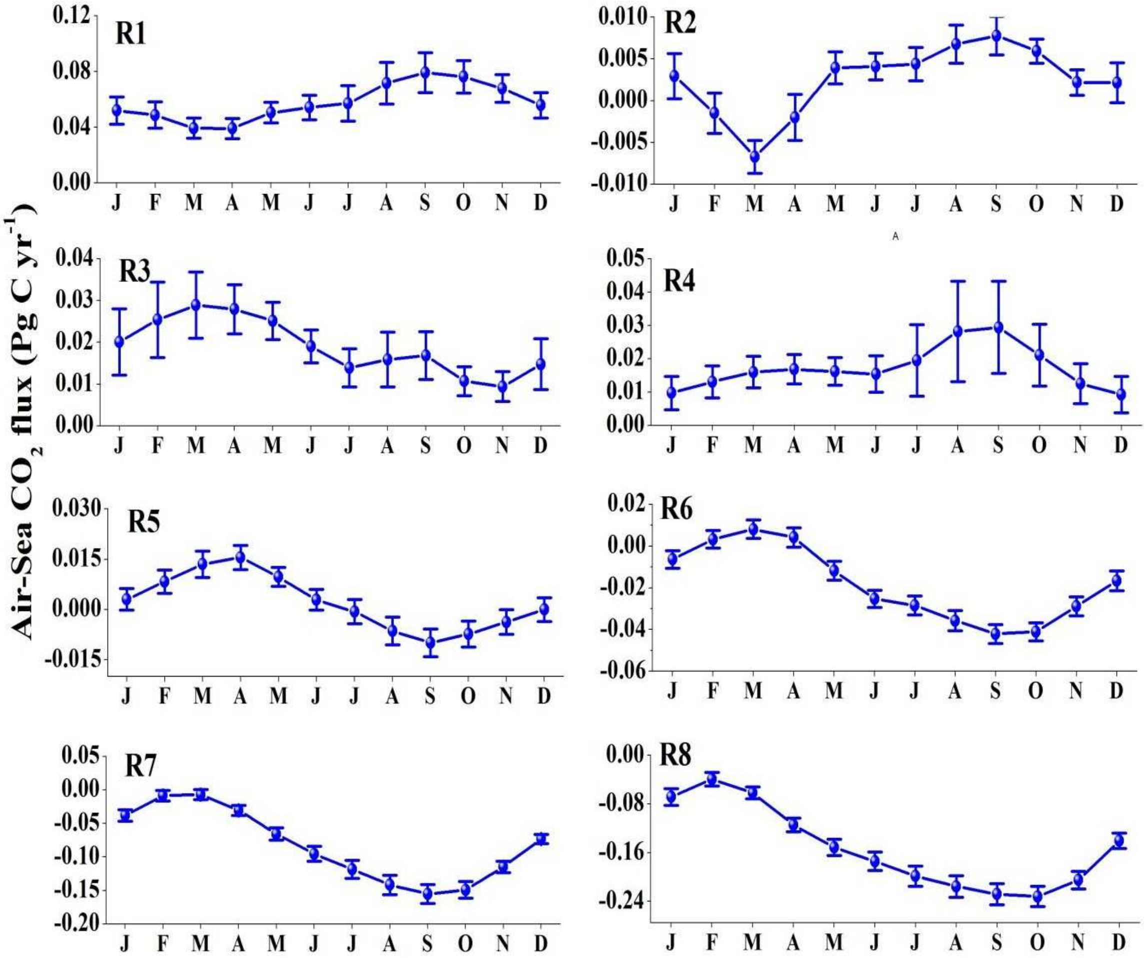

Figure 4. The seasonal cycle of area integrated sea-to-air CO$_2$ flux over eight bio-provinces calculated from the assimilated sea-to-air CO$_2$ flux of Valsala and Maksyutov, (2010). The standard deviations are calculated from the interannual variability of each month of CO$_2$ flux from 1980 to 2004. Units are in Pg C yr^{-1}.

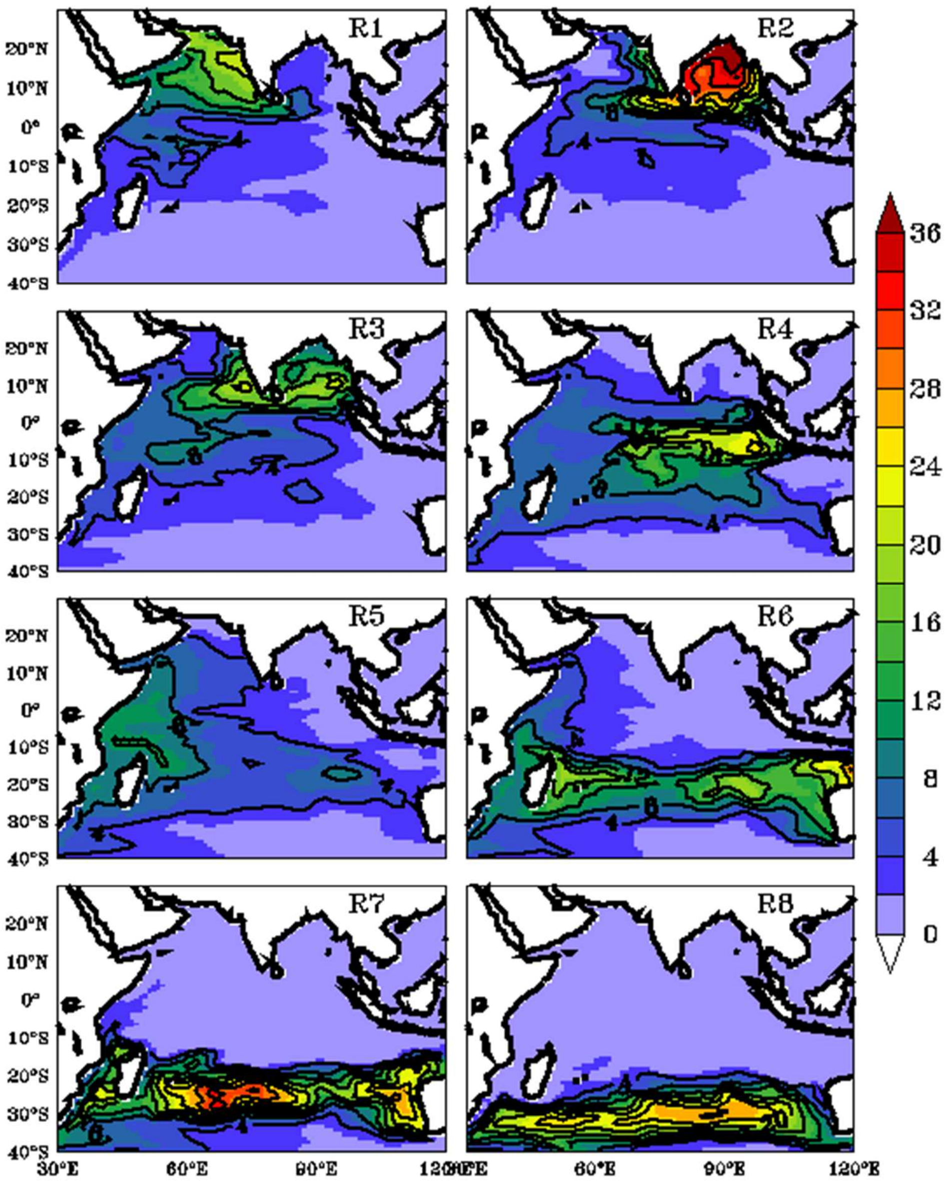

Figure 5. RMSE of dissolved inorganic carbon (DIC) for a given perturbation of 1 Pg C sink over each bio-provinces injected for all months and produced for the last year of the model output. Units are in µmol kg^{-1}.

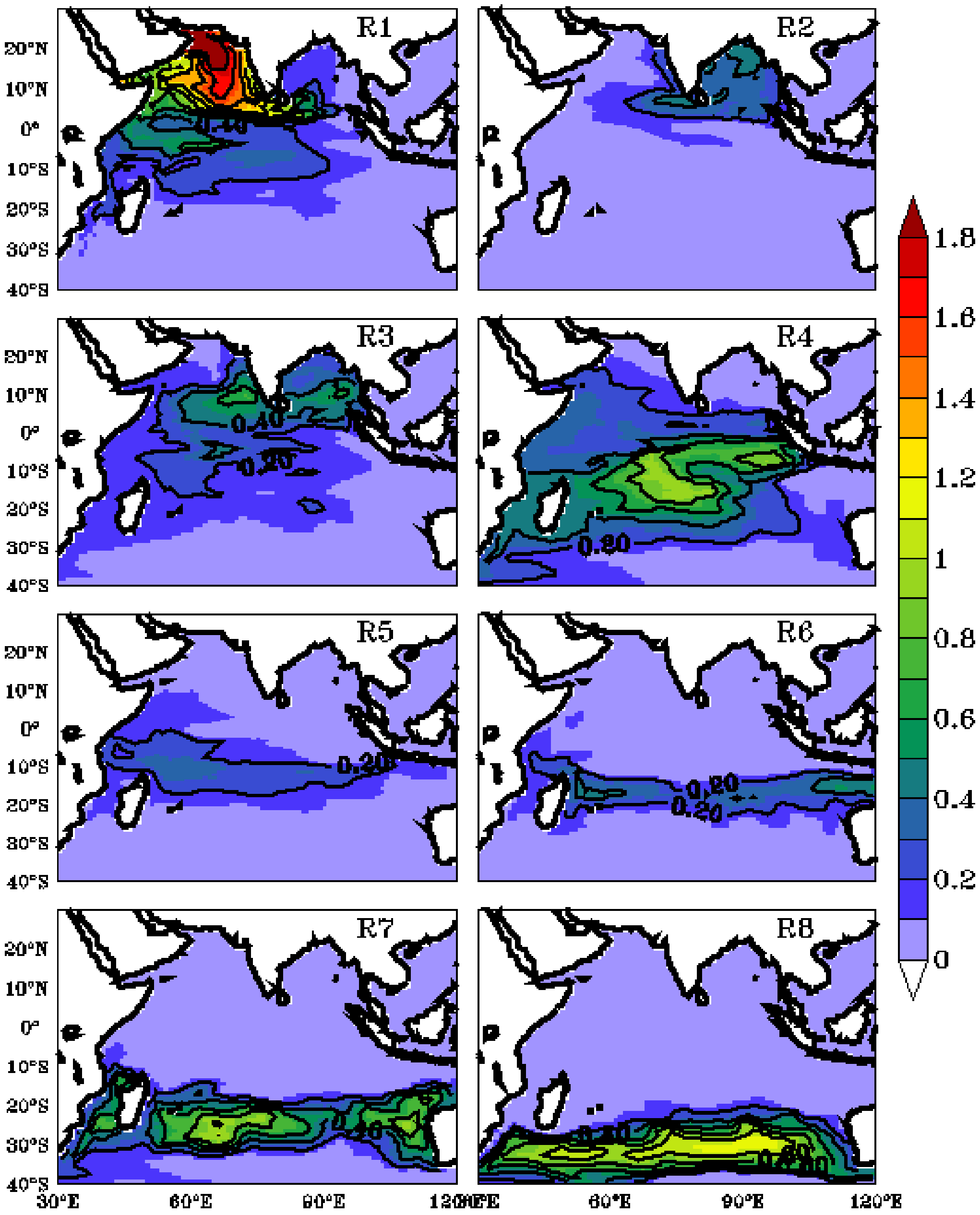

Figure 6. RMSE of dissolved inorganic carbon (DIC) for the given error perturbations in the fluxes over each bio-provinces (see text for details). The values at mooring locations are used to construct the observational error variances in the inversion. Error perturbation is given as the standard deviation of CO_2 flux for each bio-provinces for each month. Units are in μmol kg^{-1}.

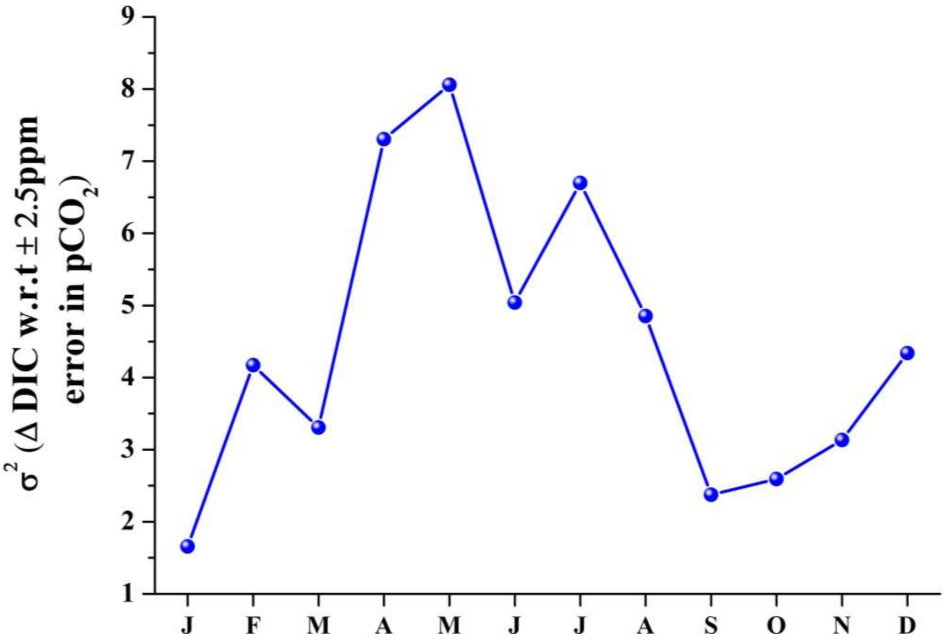

Figure 7. The seasonal cycle of observational error variances implied in the inversion at a mooring location at the central Arabian Sea (65°E, 15°N) is shown as an example. Units are in (µmole kg^{-1})^2.

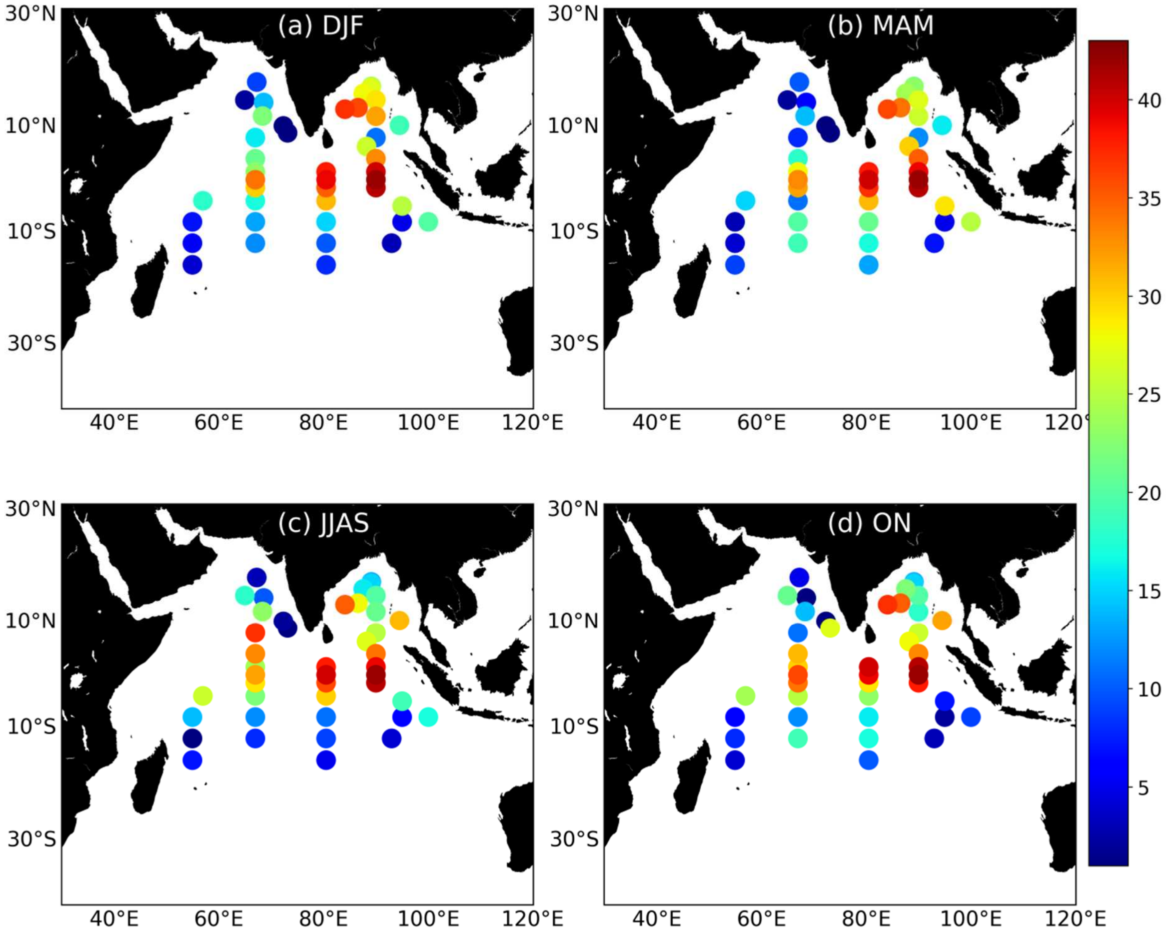

Figure 8. (a-d) Rank of RAMA+OMNI moorings identified for each season for surface ocean pCO_2 observation with deep blue (red) represents best (least) valued mooring for pCO2 observations from this OSSE experiment.

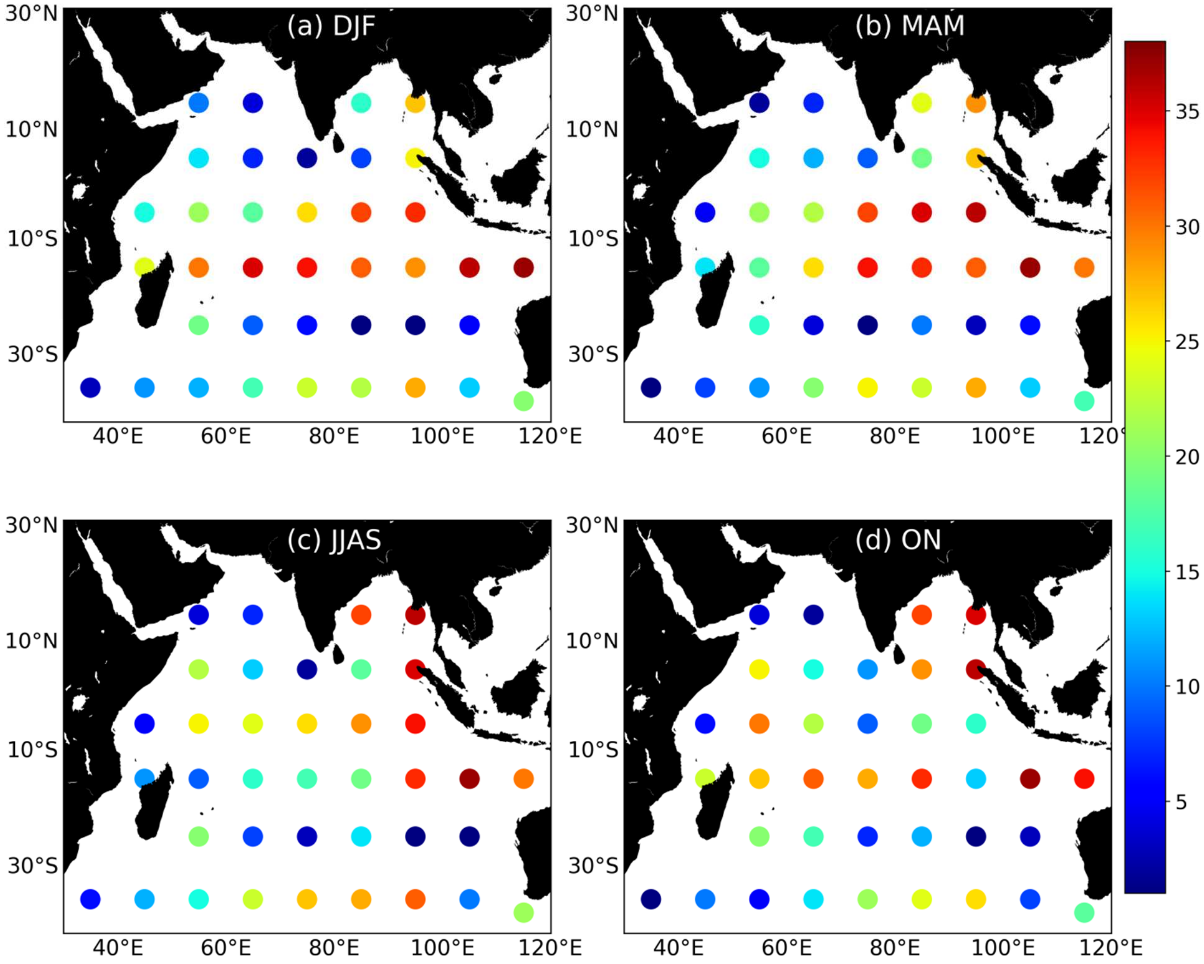

Figure 9: Same as Figure 8 but for Bio-Argos deployed at regular 10°x10° intervals.

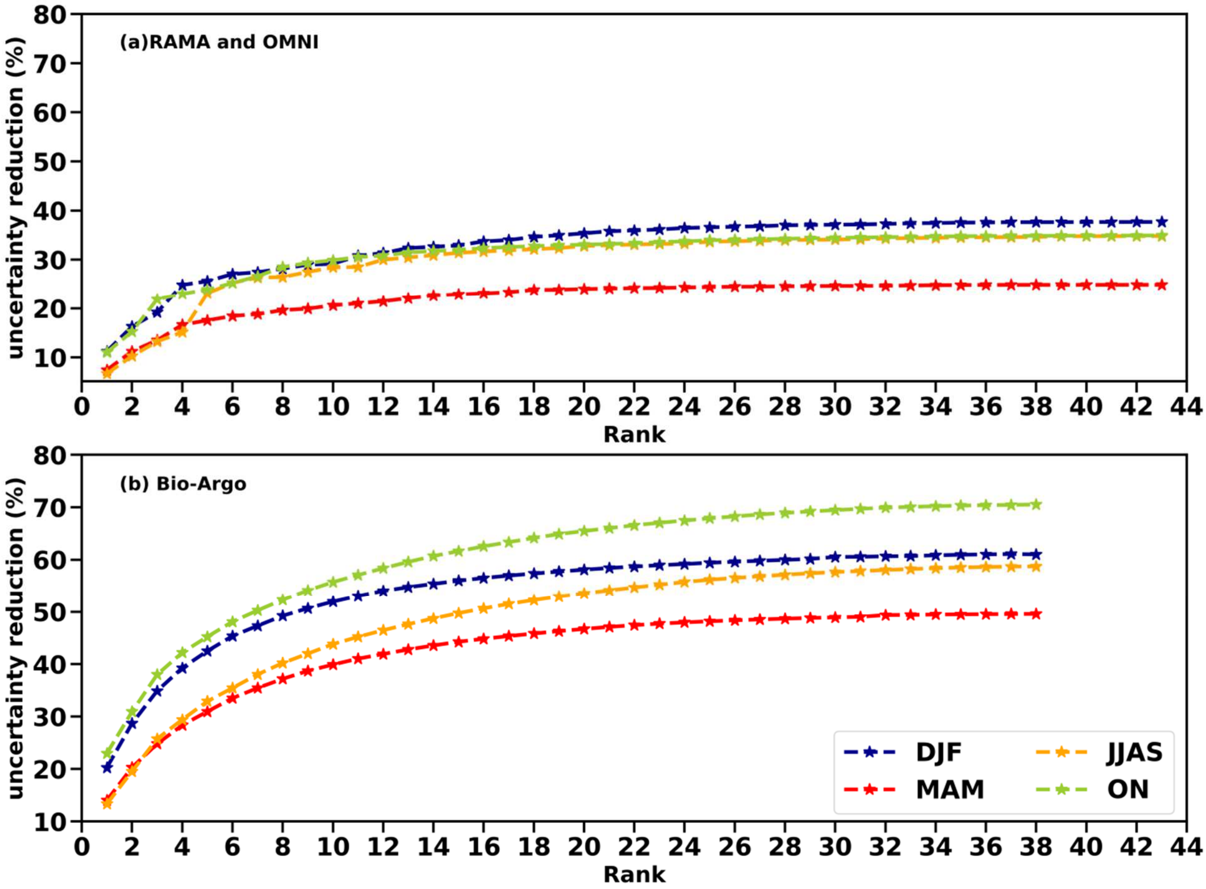

Figure 10: The percentage uncertainty reduction (UR) of (a) RAMA+OMNI moorings and (b) Bio-Argos.

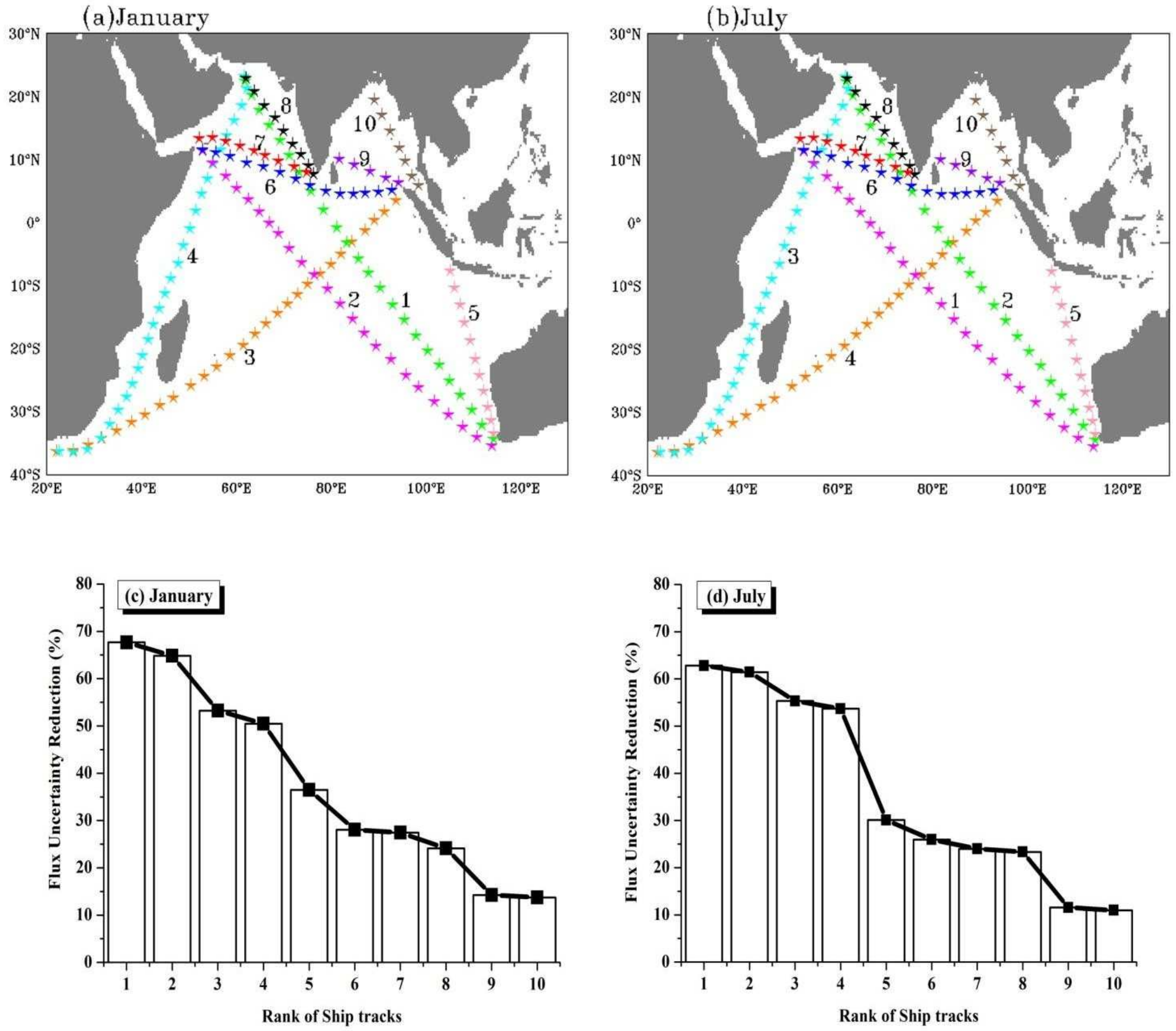

Figure 11. (a-b) The ship tracks are indicated with star symbols. The colors are given for discerning various tracks. The rank of each track in total UR of sea-to-air CO_2 fluxes during January and July are written close to the tracks. (c-d) Corresponding CO_2 flux UR (in %) corresponding to each rank.

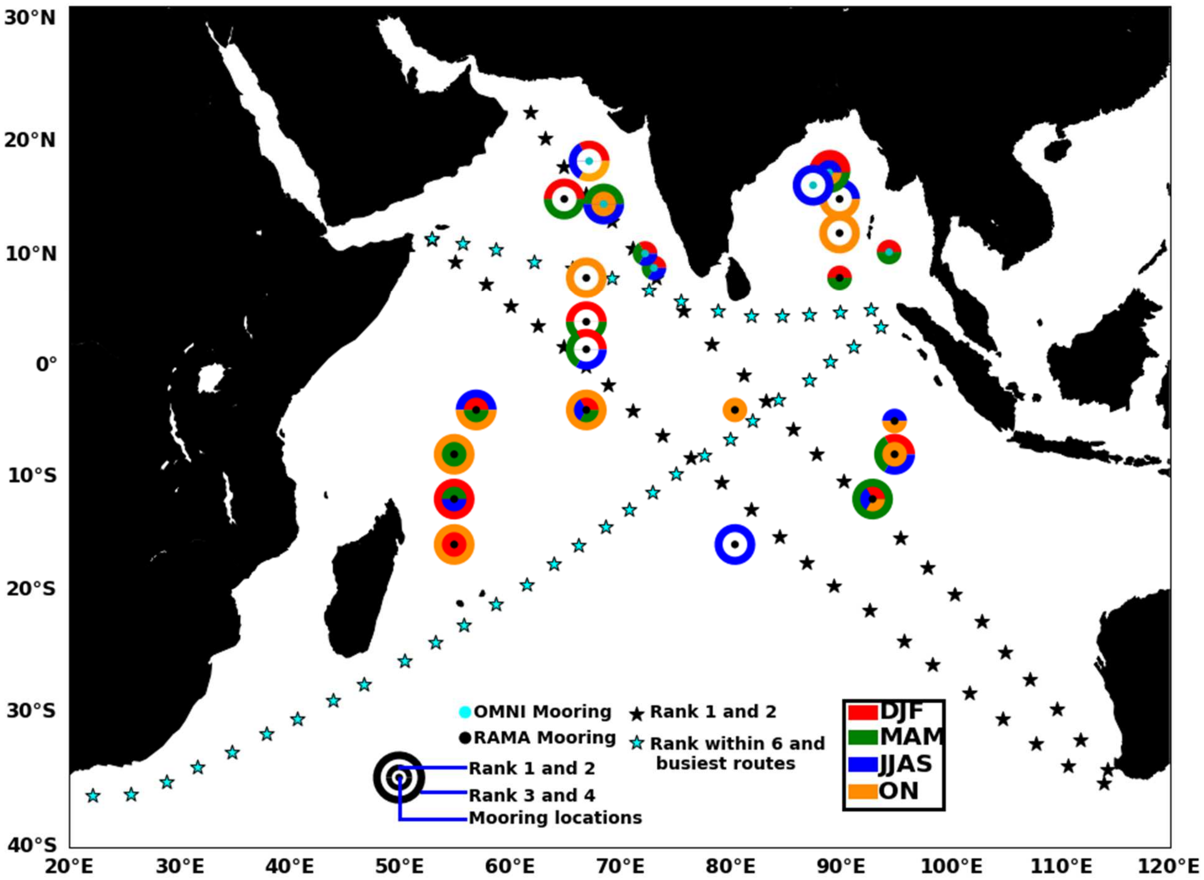

Figure 12: Locations of recommended RAMA+OMNI moorings and SOOP ship-tracks by the OSSE for the surface ocean pCO_2 measurements. The moorings are selected based on the ranks within the Arabian Sea, Bay of Bengal, equatorial Indian Ocean, and south subtropical Indian Ocean for all four seasons. The black dot represents mooring location, the number of circles represents a range of ranks to which each mooring belongs as re-ordered within each basin, and different seasons are indicated in different colors. The star dots represent the recommended SOOP ship-tracks.